Investigation of the strangeness baryon interaction by Λ hypernuclear spectroscopy

A pre-document for the experimental readiness review of
E12-15-008, E12-19-002, and E12-20-013.

by

F. Garibaldi, T. Gogami, P. Markowitz, S. Nagao,
S. N. Nakamura, J. Reinhold, L. Tang, G. M. Urciuoli

on behalf of JLab Hypernuclear Collaboration

This document is submitted to JLab for official request of supports
by the JLab Hypernuclear Collaboration
November 13, 2022

Abstract

Precise spectroscopy of Λ hypernuclei with the $(e, e'K^+)$ reaction has been developed and established at JLab Hall-C and Hall-A. The hypernuclear masses were deduced by the missing mass technique with measured kaon.

In Hall-C, a short orbit high-resolution kaon spectrometer (HKS) and electron spectrometer (HES) which were dedicated to hypernuclear study were introduced and low energy beam was used to achieve high resolution. In Hall-A, a pair of high-resolution spectrometers (HRS), which can measure high momentum particles, were used with higher energy beam energy which enables better signal-to-noise ratio. Two hypernuclear collaborations at JLab were merged to the JLab hypernuclear collaboration and we designed a new experiment which picks up better parts of both.

We proposed a campaign of experiments, E12-15-008, E12-19-002, and E12-20-013 which use HKS as the kaon spectrometer and HRS as the electron spectrometer with a newly introduced pair of charge separation magnets (PCS). JLab PAC44, PAC48 and PAC49 approved these experiments.

PCS was designed and constructed during COVID-19 pandemic in Japan and shipped to JLab in February, 2022.

Taking beam availability at Hall-A into account, we start exploring a possibility to perform the experiments in Hall-C rather than Hall-A. In Hall-C, HRS spectrometer cannot be used and thus we need to re-design the experiment. In this document, the modification plan and the expected performance will be described. As described in this document, we have concluded that a hypernuclear experiment in Hall-C is feasible with supports of JLab. With such supports, we hope to realize the experiments in Hall-C at the earliest opportunity.

Contents

1 Introduction

1.1 Why is hypernuclear study necessary?

Nuclear physics has the major goal of understanding the nature of many-body systems whose dynamics is dictated by the strong interaction. In the universe, there is a hierarchy of three such systems: 1) baryons and mesons, the bound systems of quarks, 2) nuclei, the self-bound systems of baryons and 3) neutron stars, isospin-asymmetric nuclear matter bound by gravitational effects. The size scale of 1) and 2) is femtometers and that of 3) is 10 km. Though they differ by 10^{19} order of magnitudes, the interactions governing their structure and properties are the same. The strong interaction in the low energy region where quantum chromodynamics (QCD) is not perturbative has been investigated in the framework of baryon potential models. The construction of NN potentials has taken advantage of the availability of a substantial number of scattering data. High-precision potential models fit all these data with extreme accuracy. However, when only two-body forces are accounted for, light nuclei turn out to be under-bound and the saturation properties of infinite isospin-symmetric nuclear matter are not correctly reproduced. This indicates the need for a three-body interaction. The same theoretical framework could be extended to the strange sector. Though the strange quark is heavier than the u and d quarks, it is still lighter than the QCD cut-off ($\approx$1 GeV) unlike the heavy quarks (c, t, b). Hence, the strange quark can be treated in the framework of the flavor SU(3) symmetry which is a natural extension of the isospin symmetry for ordinary nucleons. To devise a unified description of the baryonic interaction within the flavor SU(3) basis, one must then quantitatively understand the hyperon-nucleon (YN) and the hyperon-hyperon (YY) interactions. Spectroscopic investigation of Λ-hypernuclei, nuclear many-body systems containing one Λ particle, provides a unique and, currently, the only practical tool to study the ΛN interaction. Direct ΛN scattering experiments are technically very difficult.

While several models of YN forces were proposed in the past, recent observation of neutron stars with masses of $2M_{\odot}$ (two solar masses) poses several important questions. There is a very simple argument to justify the appearance of strange degrees of freedom in the inner core of a neutron star. In the pure neutron matter case, whenever the chemical potential becomes sufficiently large to match the chemical potential of a hyperon in the same matter, the hyperon becomes stable since it is a distinguishable particle, and creates its own Fermi sea, thereby lowering the kinetic energy of the system. This results in a so-called "softening" of the equation of state, due to a decrease of the Fermi pressure. In turn, a soft equation of state predicts a lower sustainable mass for a neutron star. So far, existing YN interactions typically predict a maximum mass no larger than $1.5M_{\odot}$, in strong contrast with the astrophysical observations (the "hyperon puzzle"). The key for solving this apparent contradiction is a more repulsive YN interaction, which increases the hyperon chemical potential, moving the onset of hyperons at higher densities. Most models

nowadays agree on this aspect, but additional constraints are needed and they can only be inferred from accurate spectroscopic data of hypernuclei.

The relation between hypernuclei and matter inside a neutron star is not straightforward. In particular, one has to remember that neutron stars are indeed 90% made up by neutrons. Hypernuclei, instead, have a neutron fraction not exceeding 60%. It is clear that the effect of asymmetry of the nuclear medium on the hyperon chemical potential (which can be for instance translated into an isospin dependence of YNN interaction) cannot be effectively constrained from the existing hypernuclear data, unless very accurate measurements on asymmetric hypernuclei are performed. Tiny changes in the binding energy, and consequently on the determination of the YN/YNN force, can have dramatic consequences on the Equation of State (EoS) of matter at supra-saturation conditions.

Another interesting aspect of the isospin dependence of the YN interaction is the charge symmetry breaking (CSB). Recently decay-pion spectroscopy of electro-produced ${}^{4}_{\Lambda}$H, which was originally proposed at JLab [**?**], was successfully carried out at Mainz [6] and the excitation energy of ${}^{4}_{\Lambda}$He 1^+ state was also successfully measured by gamma-spectroscopy at J-PARC [7]. These new experimental data strongly support the fact that the A=4 hypernuclear iso-doublet has a large CSB for the ground states (0^+) and small CSB for the excited 1^+ states. Although the origin of such a large CSB is not fully understood, it is clear that the discussion based on 2-body YN/NN interaction only does not suffice and that the inclusion of $\Lambda N - \Sigma N$ coupling and 3-body forces are essential. For heavier and more neutron rich hypernuclear systems, such $\Lambda N - \Sigma N$ coupling and 3-body forces become more important, implying that the behavior of Λ in symmetric nuclear matter and neutron-rich environments would be quite different. The accuracy of existing hypernuclear data is not adequate to test the features of the baryonic force models needed to properly address the hyperon puzzle, and thus higher precision data are necessary. It should be noted that a systematic study of Λ hypernuclei with sub-MeV accuracy over a wide mass range is quite important to solve the hyperon puzzle; the approved experiments E12-19-002 for light hypernuclei [19], E12-15-008 for medium-heavy hypernuclei [20], and E12-20-013 for a heavy hypernucleus [21] provide such precious experimental data.

1.2 Why is the JLab hypernuclear project unique?

Traditionally, meson beams have been used to study Λ hypernuclei. The $n(K^-, \pi^-)\Lambda$ reaction is a quark exchange reaction and the $n(\pi^+, K^+)\Lambda$ reaction is an $s\bar{s}$ pair production reaction; they convert neutrons into Λ particles. On the other hand, the $p(e, e'K^+)\Lambda$ reaction is kinematically similar to the $n(\pi^+, K^+)\Lambda$ reaction, but $p(e, e'K^+)\Lambda$ converts a proton to a Λ. We can see that $p(e, e'K^+)\Lambda$ and $n(K^-, \pi^-)\Lambda$, $n(\pi^+, K^+)\Lambda$ reactions produce different hypernuclei on the same target. They are complementary, and it is important to use both electron and meson beams to study the isospin dependence and charge symmetry breaking of the hypernuclei. However, sub-MeV resolution can be currently achieved with only with the electron beams thanks to high quality primary beam.

1.3 Brief history of JLab hypernuclear experiments

1.3.1 Previous hypernuclear experiments with the $(e, e'K^+)$ reaction

The $(e, e'K^+)$ reaction spectroscopy of Λ hypernuclei is based on the missing mass technique to achieve sub-MeV resolution and thus momentum vectors of scattered electrons (e') and kaons (K^+) should be measured with resolution of $|\Delta p/p| < 1 \times 10^{-4}$.

The pilot experiment to proof the principle of the $(e, e'K^+)$ hypernuclear experiment was carried out with existing spectrometers, the SOS for the kaons and the ENGE split-pole spectrometer for the scattered electrons, at JLab Hall-C (E89-009) in 2000 [8, 9]. The E89-009 experiment successfully proved the potential of the $(e, e'K^+)$ hypernuclear spectroscopy of Λ hypernuclei, however, resolution was limited by the existing spectrometers. Therefore, a kaon spectrometer dedicated to the hypernuclear spectroscopy, HKS was introduced in E01-011 [10] and an electron spectrometer, HES was introduced with an optimized configuration in E05-115 [11, 12, 13, 14]. The spectroscopic study of ${}^{7}_{\Lambda}$He, ${}^{9}_{\Lambda}$Li, ${}^{10}_{\Lambda}$Be, ${}^{12}_{\Lambda}$B was successfully performed and the spectroscopic research of Λ hypernuclei with the $(e,' K^+)$ reaction was established.

While spectroscopy of Λ hypernuclei with electron beams was in progress in Hall-C, another set of experiments were performed in Hall-A in parallel.

In Hall-A, the missing mass spectroscopy was performed by measuring scattered electrons and K^+ mesons using two HRSs, which are permanently installed vertical bending magnetic spectrometers in Hall-A. Spectroscopic study of ${}^{9}_{\Lambda}$Li, ${}^{12}_{\Lambda}$B, ${}^{16}_{\Lambda}$N was successfully carried out (E94-107) [15, 16, 17, 18].

Although the basic principle of both experiments is the same, the Hall-C experiment is characterized by lower central momentum of the scattered electron spectrometer and it results in lower beam energy. Lower momentum of the electron spectrometer enables us to achieve higher missing mass resolution if we fix the relative momentum resolution of the spectrometer. However, a special configuration of electron spectrometer is required to keep the signal-to-noise ratio reasonably high. In Hall-A, the central momentum of the electron spectrometer is much higher than the Hall-C kinematics due to higher maximum momentum of HRS. It enables us to achieve better signal-to-noise ratio since the high-rate electron background is Lorentz boosted to forward angles.

1.3.2 Coming experiments

Combining the activities of hypernuclear research at JLab Hall-A and Hall-C, the JLab hypernuclear collaboration was created and proposed new experiments [19, 20, 21].

Though we originally proposed these three experiments assuming that the experiments would be performed in Hall-A, the experiments can be carried out at Hall-A or Hall-C. In Hall-A, we can use one HRS as the spectrometer for the scattered electrons. It is a vertical bending type spectrometer and it can measure high momentum electrons with an excellent momentum resolution of $\Delta p/p \sim 3 \times 10^{-4}$. Therefore, we can use the electron beam of $E_e = 4.5$ GeV and HRS with a central momentum of $E_e = 3.0$ GeV which makes the virtual photon energy as $E_{\gamma^*} = 1.5$ GeV. Higher beam energy makes the bremsstrahlung electron background Lorentz boosted to forward angles out of spectrometer's acceptances. Therefore, we can expect good signal-to-noise ratio, although absolute e momentum resolution which contributes to the missing mass resolution, becomes worse. Another possibility is running the experiment in Hall-C with the HES as the scat-

tered electron spectrometer. HES was used for the previous hypernuclear experiments in Hall-C and it was designed to measure low energy electrons of less than 1 GeV. Therefore, the incident electron beam energy is limited to be less than 2.5 GeV if $E_{\gamma^*} = 1.5$ GeV is kept. Lower energy of scattered electrons is favored for better energy resolution since smaller momentum (p) gives better absolute resolution for the fixed relative momentum resolution $\Delta p/p$, however, it is disfavored in terms of the signal-to-noise ratio.

In order to avoid physical interference between the forward located kaon and electron spectrometers, we will install a new pair of charge separation magnets (PCS) in both Hall-A and Hall-C options. Introduction of PCS minimizes effects from the magnetic field to the unused electron beam while the previously used single large dipole (SPLitter) bent the electron beam as well as separated positively charged K^+ and negative e'. Furthermore, the single dipole magnet coupled the kaon spectrometer and the electron spectrometer beam optically. It resulted in very complicated beam tune and analysis.

Another challenge in the Hall-C option is that both HES and HKS are horizontal bending spectrometers which have no vertex resolution along the beamline. It was not a disadvantage for thin solid targets which were used in previous Hall-C experiments since these solid targets' (material) thicknesses were $\sim$ 100mg/cm^2 or less than $<$ 1 mm. Therefore, we know the reaction point along the beamline with an accuracy of $<$ 1 mm. However, we will use a gaseous target with a length of 20 cm in the new experiment and the reaction point information is necessary for the high-resolution spectroscopy. Therefore, we plan to modify the HES to be a vertical bending type spectrometer as discussed in the following sections. Based on the preliminary simulations, the solid angle of a vertical HES with the PCS is slightly reduced but the optical nature will not be drastically affected. Considering the advantages and disadvantages of the spectrometers' performance and the JLab's experimental allocation plan in Halls A and C, we chose to perform the experiments in Hall-C.

1.4 What's contained in this text?

After this introduction, we will describe the detail of PCS magnets to be installed in the coming experiments (Section 2).

Expected performance of the PCS and vertically modified HES based on simulation will be discussed in section 3.

Finally, we will list up the request of supports to JLab at the end of this text (section 6).

2 A new pair of charge separation magnets PCS

2.1 Function

The differential cross section for the (γ^*, K^+) reaction is larger at the forward scattering angle with respect to the virtual photon ($\theta_{\gamma K}$). In addition, the virtual photon flux becomes larger as the scattering angle of e' ($\theta_{ee'}$) is smaller. Therefore, detection at the smaller angles for both $\theta_{ee'}$ and $\theta_{\gamma K}$ makes the hypernuclear yield larger. A charge separation magnet is installed in front of magnetic spectrometers for scattered electrons and K^+'s in order to maximize the hypernuclear yield, avoiding physical interference of the magnetic spectrometers. In the present experiment, a pair of charge-separation dipole magnets (PCS) is used instead of the single Splitter Magnet (SPL) that we used in the previous experiment E05-115.

PCS does not create a magnetic field at the very forward angle so that e^- and e^+ backgrounds generated by electromagnetic shower processes in a target material do not lead to serious counting rates for particle detectors. Figures 2.1 and 2.2 show schematic drawings of PCS.

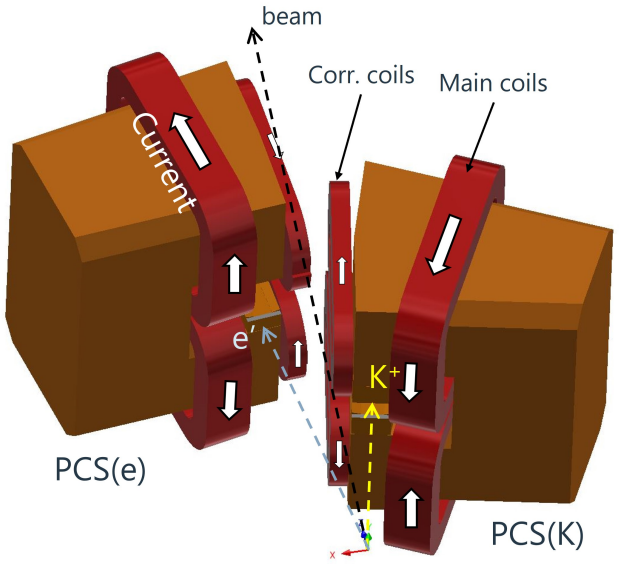

Figure 2.1: Schematic of a pair of charge-separation dipole magnets (PCS). PCS does not create a magnetic field at the forward angle so that huge amount of e^- and e^+ events do not lead to serious counting rates for particle detectors.

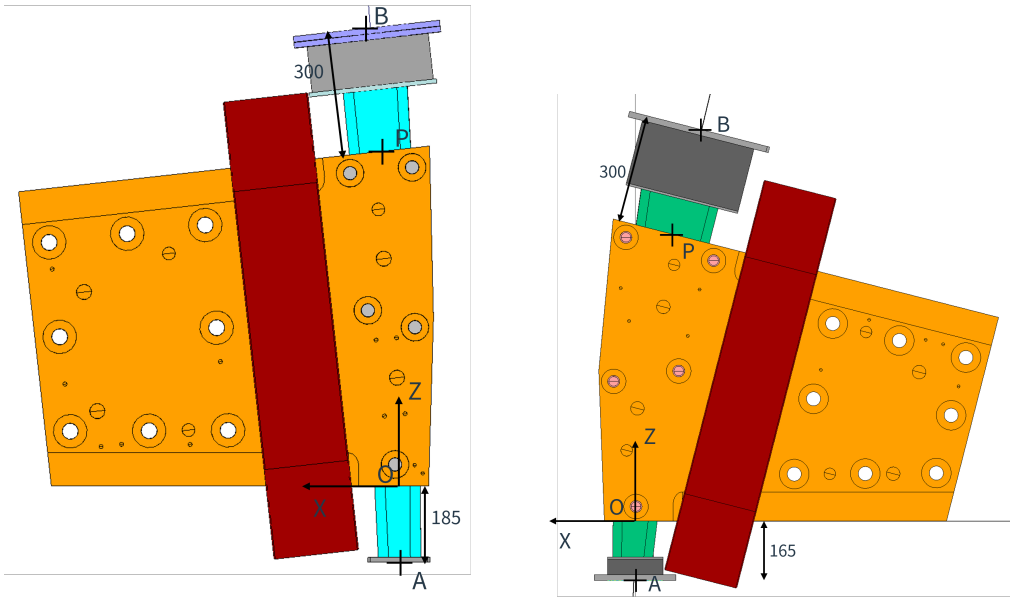

(a) PCS(e) (b) PCS(K)

Figure 2.2: Top views of the PCS(e) and PCS(K) which are C-type dipole magnets for e' and K^+.

2.2 Specifications

PCS has two C-type dipole magnets, PCS(e) and PCS(K), which are used for the e' and K^+ sides. Each magnet has main and sub coils as shown in Fig. 2.1. The sub coils reduce the magnetic flux leakage from the yokes, and thus the field in the pole gaps stays high while the stray field along the beam line is minimized. Maximum currents for the main and sub coils are 1700 and 1000 A, respectively. Basic specifications are summarized in Tab. 2.1.

Table 2.1: Basic specifications of PCS.

Items		PCS (e)	PCS (K)
Weight (/ton)		7.8	8.0
Maximum field (/T)		1.3	
Main coil	Number of turns	96	
	Maximum current (/A)	1700	
	Maximum voltage (/V)	106	
	Temperature rise (/K)	20	
Sub coil	Number of turns	88	
	Maximum current (/A)	1000	
	Maximum voltage (/V)	97	
	Temperature rise (/K)	11	

2.3 Magnetic field measurement

The magnetic field was measured by a Hall probe at the company TOKIN where the PCS was constructed. Figure 2.3 shows a photograph from when the PCS(e) and PCS(K) magnets were constructed in TOKIN.

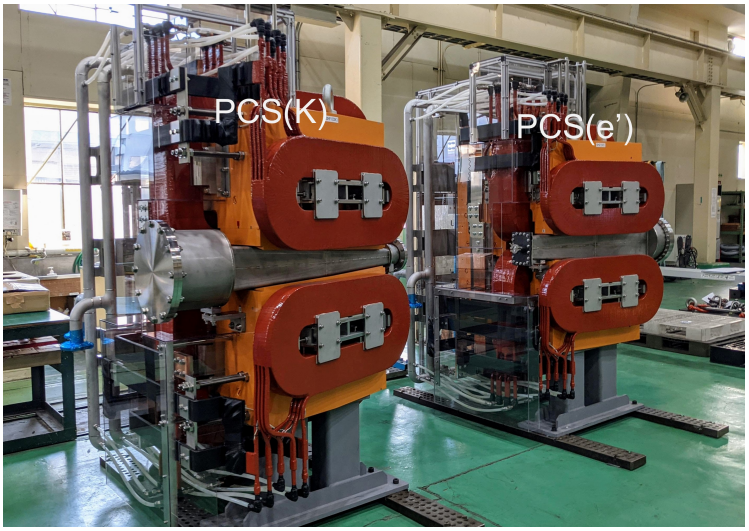

Figure 2.3: A photograph of PCS magnets.

Results of the field measurement are shown in Figs. 2.4 and 2.5 which are a B-I curve and a field map along the central ray. A 3D magnetic field was calculated by Opera3D(TOSCA). The 3D-field map is implemented into a Geant4-Monte Carlo (MC) simulation for various estimations. A model in the TOSCA calculation was modified so as to be consistent with the measurement. As a result, a difference of the TOSCA calculation from the measured field became within a %, which is fairly good enough to prepare an initial transfer matrix for a momentum analysis.

2.4 Current status

PCS has been transported to JLab early this year, and is now being stored at ESB.

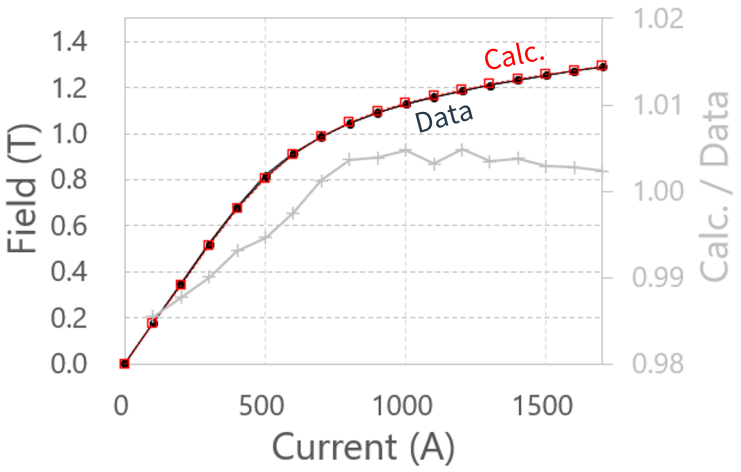

Figure 2.4: B-I curve of PCS(K). Magnetic field was measured with a Hall probe mounted at the center of the magnet under the main-coil operation (black line). TOSCA model calculation shows a red curve. A ratio of the calculation to the measurement is shown by a gray line.

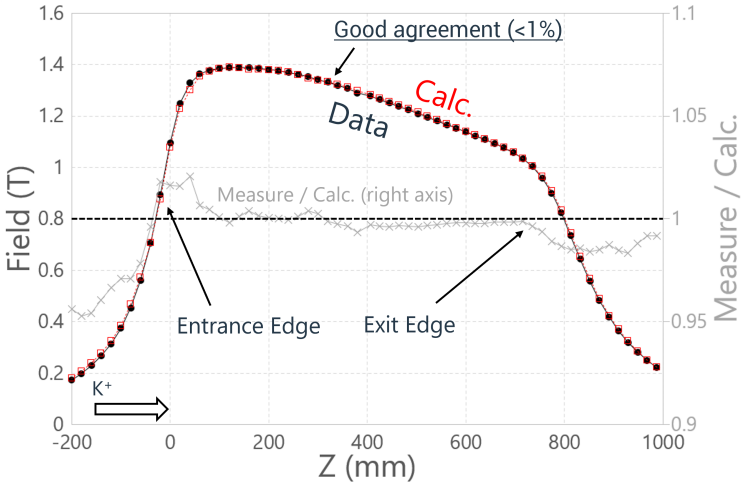

Figure 2.5: Magnetic field along the central-ray of PCS(K) as a function of the path length. Measurement and calculation are shown by black and red lines, respectively. The ratio of the measurement to the calculation is shown by a gray line.

3 Performance

Performance was evaluated by simulations based on a framework of Geant4.

3.1 Assumed configuration

An assumed setup is a combined system of vertical HES (v-HES) and horizontal HKS at JLab's Hall C. PCS is installed in front of the spectrometers to bend particles at more forward scattering angles into the spectrometers, leading to better yield of Λ hypernuclei.

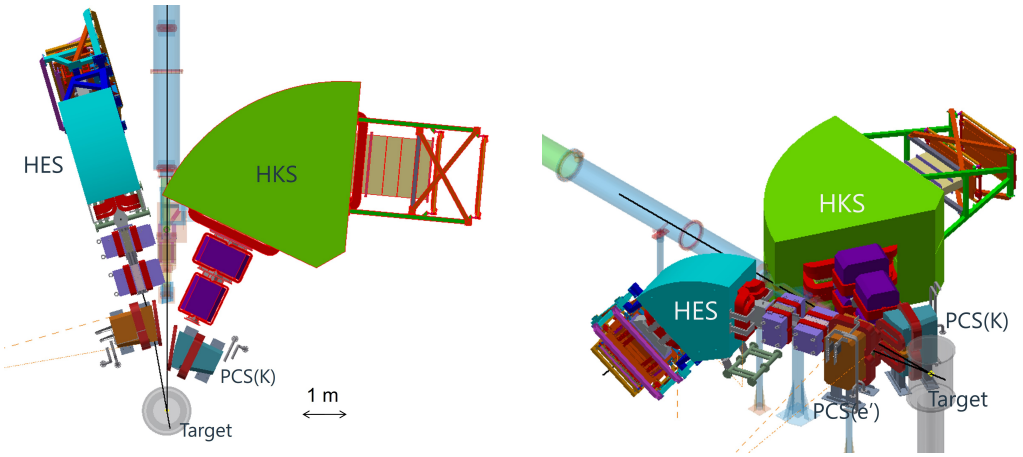

(a) Top view

(b) Bird's eye view

Figure 3.1: Assumed experimental setup is PCS + v-HES + HKS. A pair of charge-separation dipole-magnets PCS is installed between a scattering chamber, which encloses the target system, and the spectrometers (v-HES and HKS).

An incident beam at $E_e = 2.24$ GeV is transported to an experimental target. We prepare solid and gas targets shown in Tabs. 3.1 and 3.2. The experimental targets are alternately used by

Table 3.1: Experimental targets for E12-15-008 and E12-20-013.

Target	CH_2	^{6}Li	^{11}B	^{12}C	^{27}Al	^{40,48}Ca	^{208}Pb
Thickness [/(mg/cm^2)]	500	100	100	100	100	77.5	100
Hyperon/Hypernucleus	Λ and Σ^0	$^{6}_{\Lambda}$He	$^{11}_{\Lambda}$Be	$^{12}_{\Lambda}$B	$^{27}_{\Lambda}$Mg	$^{40,48}_{\Lambda}$K	$^{208}_{\Lambda}$Tl
Purpose	Calibration					Physics	

Table 3.2: Experimental targets for E12-19-002.

Target	Empty cell	Multi foil (^{12}C)	H_2	^{3}He	^{4}He
Thickness [/(mg/cm^2)]	162	100×3	54	192	262
Hyperon/Hypernucleus	N/A	$^{12}_{\Lambda}$B	Λ and Σ^0	$^{3}_{\Lambda}$H	$^{4}_{\Lambda}$H
Purpose	Calibration			Physics	

remotely moving a standard target ladder which holds the target materials and gas cells.

3.2 Simulation setup

The experimental setup was configured in the Geant4 MC simulation. Three-dimensional magnetic field, which is implemented in the MC simulation, was calculated by a software Opera3D TOSCA. TOSCA is a tool to calculate static magnetic field by using a finite element method. Simulations for PCS + v-HES and PCS + HKS are separately modeled. Outputs from the separated simulations are combined to evaluate the performance such as a missing-mass resolution and yield of hypernuclei. Figure 3.2 shows an example of viewer of the MC simulation for the PCS-HKS, in which particle tracks are seen.

3.3 Optics optimization

The magnetic field strength for each magnet needs to be optimized, considering the momentum resolution, the angle resolution, and the solid-angle acceptance. We scanned the performance by changing the magnetic field strengths to find an optimal set. Simulation results with the optimal set are shown in the following sections.

3.4 Basic specifications of spectrometer system

(1) A z-vertex resolution, (2) solid-angle acceptance, and (3) momentum resolution are described in this section.

3.4.1 Z-vertex resolution

A reaction position along with the beam direction (z direction) is necessary for the gas targets because events from the target cell needs to be removed in the analysis. The z vertex is reconstructed by a backward transfer matrix (BTM) of PCS + v-HES. Figure 3.3 shows a difference between assumed and reconstructed positions in the z direction. The FWHM of the z position distribution is 16 mm.

3.4.2 solid angle

Figure 3.4 shows the solid angle acceptance as a function of particles' momenta. The solid angle for each spectrometer was evaluated to be 4 and 8 msr, for v-HES and HKS, respectively, at the central momentum.

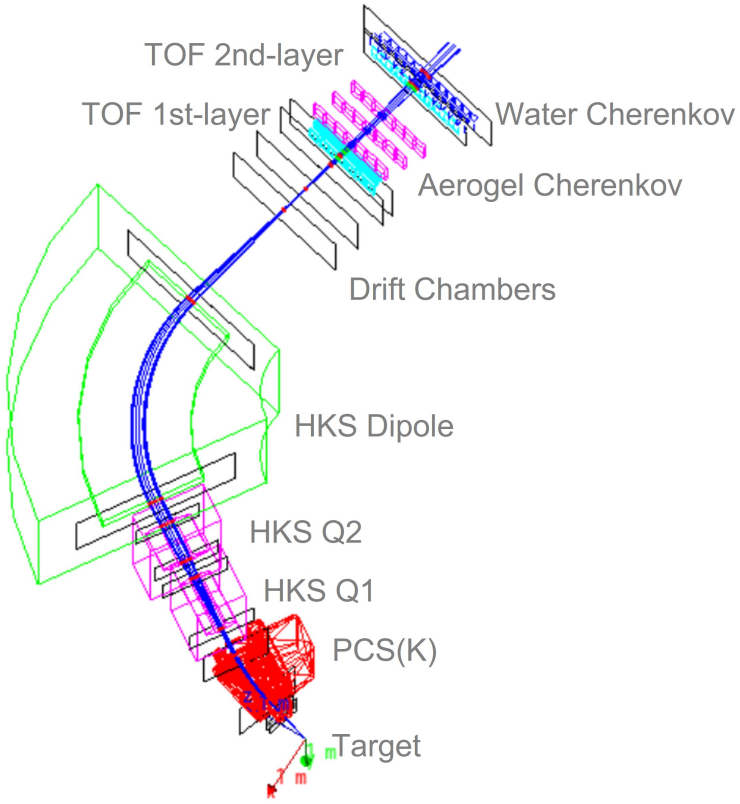

Figure 3.2: Particle tracks displayed in the Geant4 MC simultion for PCS + HKS. The simulation model contains all HKS components such as magnets and particle detectors. Blue lines show positive-charged particles at 1.2 GeV/c.

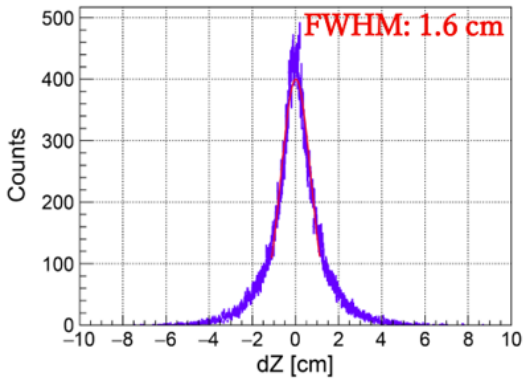

Figure 3.3: Difference between assumed and reconstructed z-vertex positions in the MC simulation of PCS + v-HES. The z-vertex reconstruction was performed by a backward transfer matrix. The width is 16 mm in FWHM when the distribution is fitted by a Gaussian function as shown.

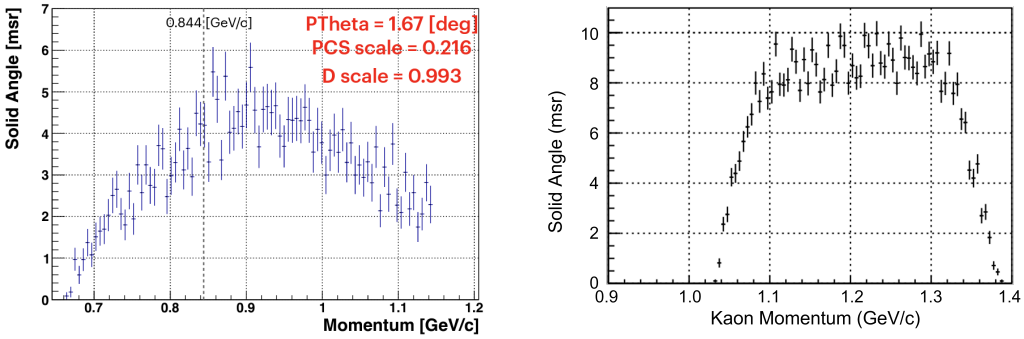

(a) PCS + v-HES (vertical bending)

(b) PCS + HKS (horizontal bending)

Figure 3.4: Solid angle acceptances as a function of the momenta.

3.4.3 MOMENTUM RESOLUTION

The momentum of particle in each spectrometer was reconstructed by using a backward transfer matrix. Figure 3.5 shows differences between the assumed and reconstructed momenta for PCS + v-HES (left panel) and PCS + HKS (right panel), respectively. The momentum resolutions were evaluated to be $\Delta p/p \simeq 6 \times 10^{-4}$ and 3×10^{-4} in FWHM for v-HES and HKS, respectively.

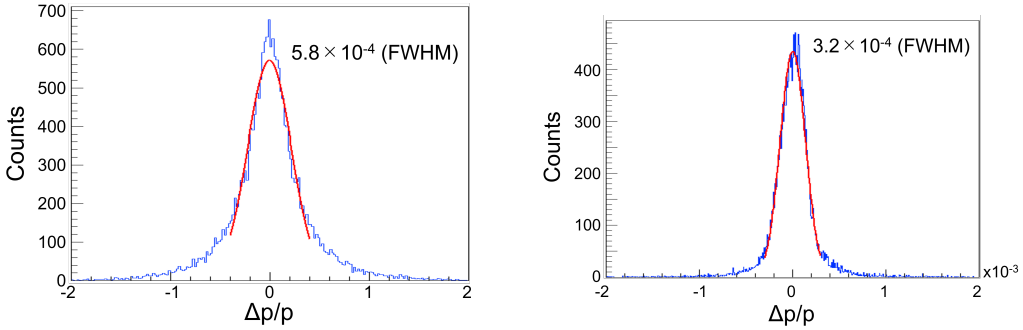

(a) PCS + v-HES (vertical bending)

(b) PCS + HKS (horizontal bending)

Figure 3.5: Differences between assumed and reconstructed momenta for PCS + v-HES (left panel) and PCS + HKS (right panel). The momentum resolutions were found to be $\Delta p/p \simeq 6 \times 10^{-4}$ and 3×10^{-4} (FWHM) for the PCS + v-HES and PCS + HKS, respectively.

3.5 Expected results

3.5.1 Missing-mass resolution

The missing-mass resolution is evaluated to be about 0.6 MeV FWHM based on the estimated momentum and angular resolutions with the assumption of the point production. The target thickness is the order of 0.1 mm and no raster is applied for solid targets but the lead target, for which a beam raster of 3×3 mm^2 is applied. Therefore, the 0.6-MeV resolution is expected for the solid targets. On the other hand, there is the finite length of 200–220 mm in the beam direction, and the beam raster of 2×2 mm^2 is applied for the gas targets. The optical analysis by the backward transfer matrix is more complex and the resolution would be limited due to the particle production from finite volume in the case of gas targets. As a result of the MC simulation, the missing mass resolution for the gas targets is estimated to be about 1 MeV in FWHM.

3.5.2 ${}^{12}_{\Lambda}$B, ${}^{40,48}_{\Lambda}$K, and ${}^{208}_{\Lambda}$Tl productions (solid targets)

Expected hypernuclear yield could be described with

$$Y = N_t \times N_e \times \Gamma \times \frac{d\sigma}{d\Omega_{HKS}} \times \Delta\Omega_{HKS} \times \epsilon_{HES} \times \epsilon_{HKS} \times \epsilon_{decay}. \tag{3.1}$$

N_t and N_e are the number of target nuclei and the number of beam electrons, respectively. Γ and $\Delta\Omega_{HKS}$ are the virtual photon flux and the solid angles estimated by the Monte-Carlo simulation, respectively. ϵs are the efficiencies assumed by typical values of E05-115.

Expected hypernuclear yields and some assumptions for the solid targets are shown in Tab. 3.3.

Amount of an Accidental background due to the random coincidence between HKS and HES was estimated by single-rate simulation which could reproduce E05-115 results.

Figures 3.6, 3.7, and 3.8 show the expected spectra for ${}^{12}_{\Lambda}$B, ${}^{40}_{\Lambda}$K, and ${}^{208}_{\Lambda}$Tl, respectively. Hypernuclear yield of ${}^{12}_{\Lambda}$B ground state is 120 counts in 36 hours beamtime. $>5\ \sigma$ peak could be

Table 3.3: Estimated yields for the solid targets.

Hypernucleus	${}^{6}_{\Lambda}$He	${}^{11}_{\Lambda}$Be	${}^{12}_{\Lambda}$B	${}^{40}_{\Lambda}$K	${}^{48}_{\Lambda}$K	${}^{208}_{\Lambda}$Tl
Target thickness [/(mg/cm^2)]	100	100	100	77.5	77.5	100
Cross section (g.s.) [/(nb/sr)]	10	10	100	50	50	86
Beam intensity (/μA)			50			25
Beam time (/hours)	28	28	36	230	280	480
Yield (g.s.)	21	11	120	130	130	42

expected. Statistical uncertainty when the lowest-energy peaks were fitted by a Gaussian function were found to be $|\Delta B_{\Lambda}^{\mathrm{stat.}}| \sim 20$ keV. Yield of ${}^{40}_{\Lambda}$K ground state is 130 counts in 230 hours. Peak significance of the ground state peak is 3.8 σ. Yield of ${}^{208}_{\Lambda}$Tl ground state will be 42 counts in 480 hours. Peak significance of the ground state peak is 1.7 σ.

Expected yields of hypernuclei for the solid targets are less than the original expectation values in Hall-A. Our simulations show that the Hall-C experiment has better energy resolution, but the S/N ratio and hypernuclear yields are lower than them in the Hall-A experiment. Honestly speaking, it is preferable to have more statistics for all solid targets to have more hypernuclear yields and to use lower beam current to have better S/N ratio. The collaboration is now studying feasibility of multi-foil targets to have more hypernuclear yields without serious increasing of beamtime, deterioration of resolution and S/N ratio.

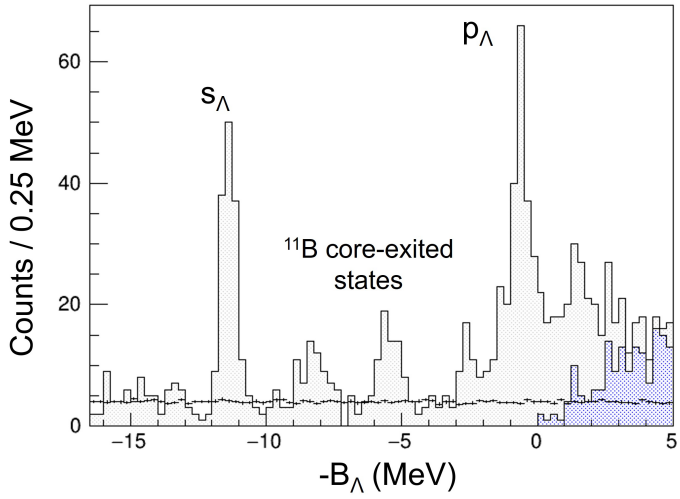

Figure 3.6: Expected binding-energy spectrum for the ${}^{12}\mathrm{C}(e,e'K^{+})^{12}_{\Lambda}\mathrm{B}$ reaction with the resolution of 0.6 MeV in FWHM. Beam time of 36 hours with the beam intensity of 50 μA is assumed.

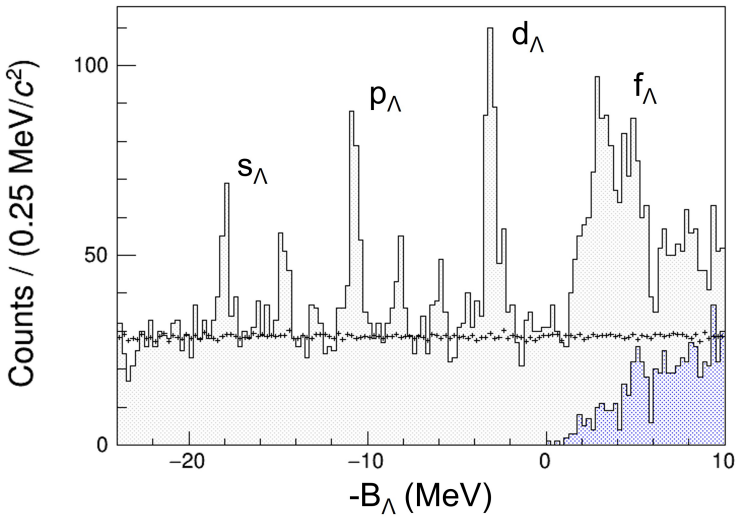

Figure 3.7: Expected binding-energy spectrum for the $^{40}\mathrm{Ca}(e,e'K^+)^{40}_{\Lambda}\mathrm{K}$ reaction with the resolution of 0.6 MeV in FWHM. Beam time of 230 hours with the beam intensity of 50 μA is assumed.

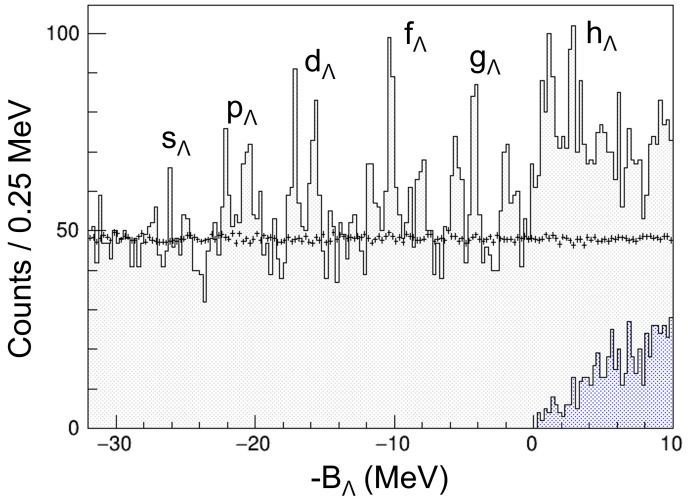

Figure 3.8: Expected binding-energy spectrum for the $^{208}\mathrm{Pb}(e,e'K^+)^{208}_{\Lambda}\mathrm{Tl}$ reaction with the resolution of 0.6 MeV in FWHM. Beam time of 480 hours with the beam intensity of 25 μA is assumed.

3.5.3 $^{3}_{\Lambda}$H and $^{4}_{\Lambda}$H productions (gas targets)

In addition to the factors used for the yield estimation of the solid targets, two additional factors need to be taken into account for the gas targets. One is a fraction of the gas density reduction due to a local heat increase by the beam exposure. The other is a survival efficiency of the signal when events from the target cell are cut by information of the reconstructed z vertex position. The factor of gas-density reduction is assumed to be 0.5 which is a conservative assumption. We assume the z-vertex resolution of 20 mm (FWHM) to be conservative as well, although the resolution was found to be 16 mm (FWHM) in the Geant4 MC simulation as shown in Sec. 3.4.1. When the survival efficiency of the signal is set to 0.8 by the z-vertex cut, the event contamination from the target cell is suppressed by 98%.

Yields for the $^{3}_{\Lambda}$H and $^{4}_{\Lambda}$H hypernuclei are about 262 and 216 assuming the beam times of 600 and 120 hours (25 and 5 PAC days), and the differential cross sections are 5 and 20 nb/sr, respectively. Figures 3.9 and 3.10 show the expected spectra for the $^{3}_{\Lambda}$H and $^{4}_{\Lambda}$H measurements, respectively.

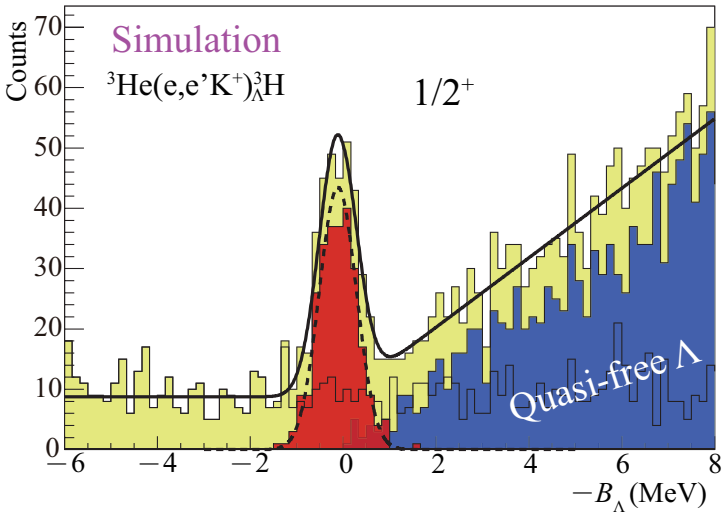

Figure 3.9: Expected binding-energy spectrum for the $^{3}\mathrm{He}(e,e'K^{+})^{3}_{\Lambda}\mathrm{H}$ reaction with the resolution of 1 MeV in FWHM. Beam time of 600 hours (25 PAC days) with the beam intensity of 20 μA is assumed. The differential cross section is assumed to be 5 nb/sr.

In Hall C, yield and S/N are expected to be worse than those of Hall A. Therefore, the beam intensity and beam time need to be optimized. Here, the beam current is assumed to be 20μA which is smaller to 1/2.5 compared with the assumption for Hall A. The beam time is 2.5 times longer to compensate the smaller current. The expected accuracy with these conditions of beam current and time is shown in Fig. 3.11. The systematic error which is evaluated to be $|\Delta B_{\Lambda}^{\mathrm{sys.}}| \simeq$ 60 keV [22, 23] is also taken into account. This choice of the beam conditions, which is one of options, reasonably achieves our original goal for the energy accuracy [24].

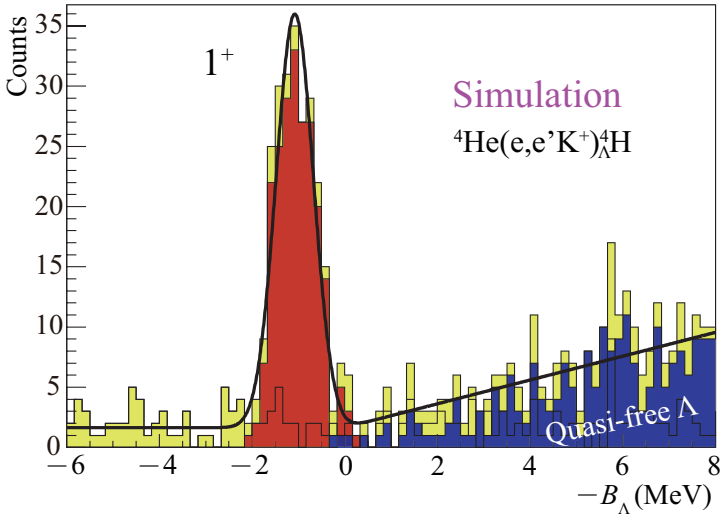

Figure 3.10: Expected binding-energy spectrum for the ${}^{4}\mathrm{He}(e,e'K^{+})^{4}_{\Lambda}\mathrm{H}$ reaction with the resolution of 1 MeV in FWHM. Beam time of 120 hours (5 PAC days) with the beam intensity of 20 μA is assumed. The differential cross section is assumed to be 20 nb/sr.

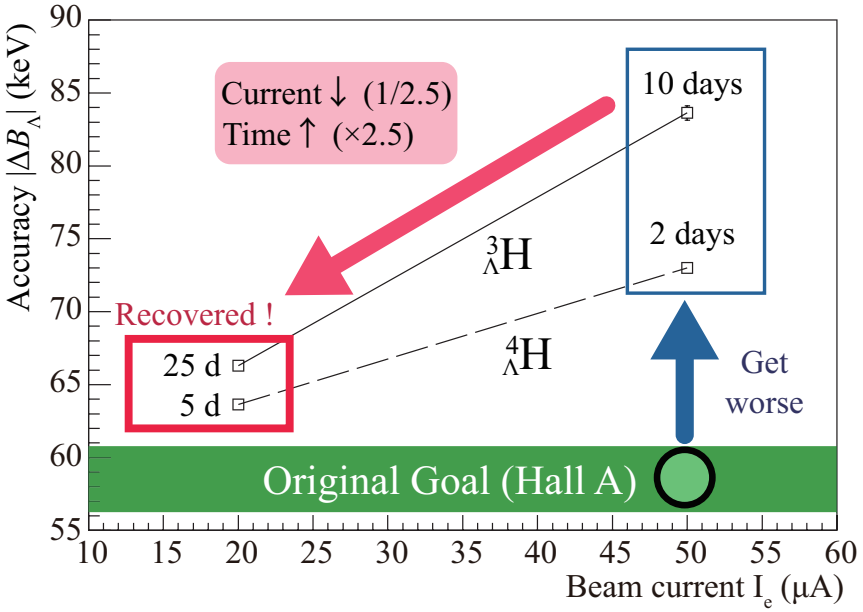

Figure 3.11: An example of how to recover the accuracy for ${}^{3}_{\Lambda}\mathrm{H}$ and ${}^{4}_{\Lambda}\mathrm{H}$ measurements. The accuracy that takes into account both statistics and systematic errors is reasonably recovered to the original goal by reducing the beam current to 1/2.5 and increasing the beam time by a factor of 2.5.

4 Detectors

We are going to use existing detectors for the HES and HKS except for water Cherenkov counters in HKS. Details of the detectors can be found in published Refs. [25, 26, 27]. Figures 4.1 and 4.2 show schematic drawings of HKS and HES detectors taken from Ref. [27]. HKS has two layers

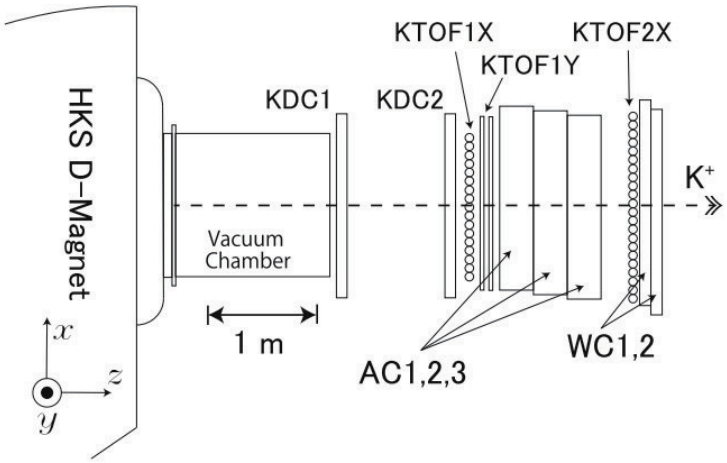

Figure 4.1: Schematic drawing of HKS detectors [27].

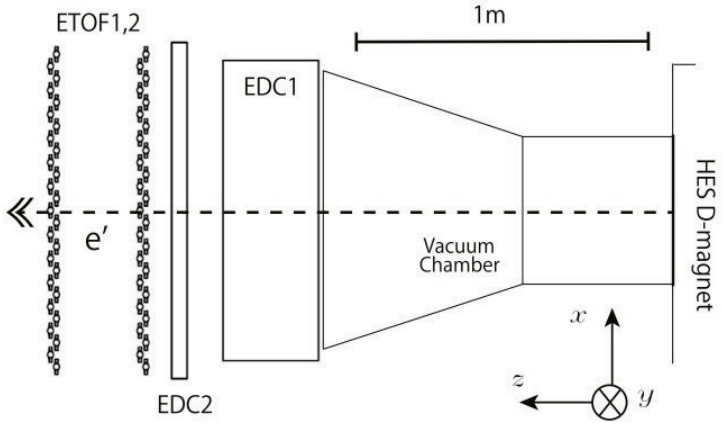

Figure 4.2: Schematic drawing of HES detectors [27].

of drift chambers for particle tracking (KDC1, 2), three layers of plastic scintillation counters (KTOF1X, 2X, 1Y) for time-of-flight measurement, and two types of Cherenkov counters (WC,

AC) for particle identification. On the other hand, HES has two drift chambers (EDC1, 2), and two layers of scintillation counters (ETOF1, 2).

The detector commissioning has already been started at ESB. AC is an aerogel Cherenkov detector which contains hydrophobic silica aerogel tiles as Cherenkov radiators. In AC, there are 21 segments which hold 42 PMTs in total. A test with cosmic rays was completed for all of the AC segments (PMTs) this year, and it was found that AC works well. Operation tests for the drift chambers and TOF counters are planned for next. The water Cherenkov counters (WC) that we used in the previous experiment will be replaced by new ones. Performance check for the new WC was completed in Japan. The new WC is going to be transported to JLab next year. Table 4.1 summarizes the preparation status of the detectors.

Table 4.1: List of detectors for the next JLab hypernuclear experiments. All detectors were used in the previous hypernulear experiments at Hall C except for water Cherenov counters (WC).

	Detector	Current status	No. of channels		Ready?
			ADC	TDC	
HKS	Drift Chambers	To be tested	N/A	360 + 360	Yes
	TOF counters	All PMTs were checked	88	88	
	Aerogel Cherenkov	Test done	42	42	
	Water Cherenkov	New boxes under construction	48	48	
HES	Drift Chambers	To be tested	N/A	1098+360	
	TOF counters	To be tested	116	116	

5 Summary of necessary modifications

5.1 Experimental setup

5.1.1 HES

The spectrometer HES used for e' measurement needs to be changed to a vertical bending system from the original horizontal bending one. This modification allows us to perform precise hypernuclear spectroscopy with gas targets for the first time at JLab. HES was designed to be used at an 8-degree tilt angle, but was not designed to rotate 90 degrees. We need full support of JLab engineer for modification of HES to a vertical bending spectrometer and design and construction of support system.

5.1.2 HKS

We assume to use HKS with the original horizontal bending configuration. However, it should be noted that a change to a vertical bending spectrometer as is applied for HES would lead to a further improvement of z-vertex analysis. The change may improve the spectroscopic quality particularly for the gas targets. On the other hand, the solid angle acceptance may be reduced due to a complicated beam-optics coupling to PCS. Therefore, a careful study of the beam optics is necessary in this case.

The water Cherenkov detector (WC) is going to be replaced by new one. Basic design and tests with cosmic rays were completed in Japan, and materials of the new WC will be soon ready for shipping to JLab.

A vacuum extension (VE) attached to the dipole magnet may need a modification. The side wall of VE generated huge amount of electromagnetic backgrounds in the previous experiment (E05-115) [27]. Positrons generated in a target hit the VE's side wall and generated secondary particles toward the detectors. The background was serious, and thus high intensity beam was not allowed for an experimental target with a large proton number. PCS is used instead of a splitter magnet (SPL) to prevent most of positrons from hitting the VE wall in the present experiments. Double-check if the PCS introduction is good enough as the treatment of positron backgrounds is on-going by the MC simulation. The side-wall material of VE would need to be changed to lighter materials if the effect of the positron background is not negligible.

5.2 Beam time estimation

The virtual photon flux is reduced by half due to the change of experimental hall which leads to the change from HRS to v-HES. For the gas target, the beam intensity may need to be reduced as shown in Sec. 3.5.3. The assumed beam intensity is smaller by 60% (50 to 20 μA), and thus, the hypernuclear yield is reduced by 80% for the ^{3,4}He targets.

The statistical accuracy for B_Λ measurement depends on statistics, S/N, and the missing-mass resolution. The missing mass resolution is expected to be 0.6 and 1.0 MeV/c^2 (FWHM) for the solid and gas targets, respectively. Table 5.1 summarizes the beam time estimation for each target to achieve reasonable results (for solid targets, more statistics is necessary to achieve original goals.)

It should be noted that beam current can be reduced if the beam time is extended to keep the yields of hypernuclei and lower beam current is preferable in terms of S/N. If further simulation study reveals that the particle rates at spectrometers are well under control, we may introduce multi-foil or thicker targets to have more statistics for solid targets. Such a study is in progress.

Table 5.1: Necessary beam time for each target to achieve original goals.

Experiment	Target (thickness /[mg/cm^2])	Beam time (/hours)	Beam current (/μA)	Remarks
E12-19-002	H gas (54) + cell (162)	60	20	calibration
	Multi ^{12}C foils (100 $\times$ 3)	100	20	
	Empty cell (162)	12	20	
	^{3}He gas (165) + cell (162)	600	20	physics
	^{4}He gas (228) + cell (162)	120	20	
	Subtotal	892		
E12-15-008	CH_2 (500)	54	2	calibration
	^{6}Li (100)	28	50	
	^{11}B (100)	28	50	
	^{12}C (100)	36	50	
	^{27}Al (100)	80	50	
	^{40}Ca (77.5)	230	50	physics
	^{48}Ca (77.5)	278	50	
	Subtotal	734		
E12-20-013	^{208}Pb (100)	480	25	physics
Total		**2106**		

6 Support request

We need official support by JLab particularly for the following items. A contact person for each item is also shown. Experimental Readiness Review (ERR) is aimed to be carried out in the beginning of 2024, although we are seeking the earliest occasion for ERR as the present experiment provides important keys to solve urgent physics issues as shown in Sec. 1.1.

1. Target System
   ⟶ Contact: **T. Gogami** (Kyoto Univ.), gogami.toshiyuki.4a@kyoto-u.ac.jp
   - **Target, ladder, cell, cryogenic system etc.**
     There are solid and gas targets used for the experiment. All targets are mounted on a linear motion system which can be remotely controlled. The ^{3,4}He gas targets, which are contained in cylindrical cells with a diameter of 200 mm, are cooled down to 12 K in operation. On the other hand, the H_2 gas target is contained in a larger cell of which diameter is 220 mm, and is cooled down to 30 K in operation. The height of each cell is 50 mm. The solid targets also need a heat sink. The conceptual design was done based on the target design for the PREX/CREX experiment. We need support for detailed design, performance test, construction, installation, and operation. Safety assessment is also necessary.
   - **Scattering chamber**
     The solid target and gas cells are installed in a scattering chamber in which the vacuum environment is realized. The scattering chamber needs to be designed considering coupling and interference with other components such as a beam line and the e' and K^+ spectrometers.

2. Radiation budget
   ⟶ Contact: **S.N. Nakamura** (Univ. of Tokyo), nue@nex.phys.s.u-tokyo.ac.jp
   Simulations to calculate the integrated dose for all the experiments (including material activation). Of particular interest is the radiation towards the Hall roof and in the detector electronic hut.

3. Magnet and spectrometers
   ⟶ Contact: **S. Nagao** (Univ. of Tokyo), sho.nagao@nex.phys.s.u-tokyo.ac.jp
   - **Base of PCS**
     A base for the new magnet PCS needs to be designed and constructed.
   - **HES modification and Spectrometers' bases**
     Modification of HES to a vertical bending spectrometer is necessary. Safe re-configuration of magnets and minimizing any effects to the optics nature of the spectrometer need

careful design. We need full supports of JLab for HES modification. A base for v-HES needs to be designed and constructed. We need JLab's supports for design and construction of HES modification and new supporting system.

On the other hand, HKS will be used as a horizontal bending spectrometer as it was. Therefore, the existing base for HKS can be used unless it conflicts with SHMS and other items in Hall-C.

- **Power supplies and cooling water**

Table 6.1: Power suuply and cooling water for PCS magents.

Coil	Item	PCS-e'	PCS-K
Main Coil	Current (/A)	1700	
	Voltage (/V)	120	
	Water (/MPa, /(L/min)	0.5, 180	
Correction Coil	Current (/A)	1000	
	Voltage (/V)	110	
	Water (/MPa, /(L/min)	0.5, 180	

Table 6.1 summarizes electric power supply and cooling water requirements for new PCS magnets. All power supplies and cooling water used for HKS and HES in the previous Hall-C experiments are necessary except for the power supply for SPL which is replaced by PCS.

Originally, we planned to use HES power supply for the correction coil and SBS power supply for PCS in Hall-A and assumed PCS-e' and PCS-K coils were connected to power supply in series. However, HES power supply is necessary for HES in Hall-C, so we need another power supply for the correction coil of PCS. It should be noted that necessary bending power for e' is reduced in Hall-C, so required current for PCS-e' will be reduced from it in Hall-A. Details of power supplies and cooling water should be optimized with the discussion with JLab experts.

- **Design of beam pipes, sieve slits etc.** Based on existing magnets drawings, designed and fabrication of beam pipes, flanges are necessary with JLab engineer. Sieve slits, collimators for the previous experiments cannot be used for the next experiments, and thus we need JLab's supports.

4. DAQ
   ⟶ Contact: **T. Gogami** (Kyoto Univ.), gogami.toshiyuki.4a@kyoto-u.ac.jp

HKS trigger system is complicated and special FPGA modules were used in the previous Hall-C hypernuclear experiments. In the next experiment, similar sophisticated trigger logic with FPGA modules are necessary. We already have a candidate for the FPGA module to be used in the trigger system, but we would like to have detailed discussion with the JLab experts to enable a smooth connection with the existing trigger system.

5. Electronics and Cabling
   ⟶ Contact: **J. Reinhold** (Florida Int. Univ.), reinhold@fiu.edu
   We are planning to use the same spectrometer system as used for the 2009 run of HKS/HES. The electronics layout for this exists.

6. Online and offline analyzers
   ⟶ Contacts: **L. Tang** (Hampton Univ.), tangl@jlab.org
   Analysis packages for HKS and HES exist already. We are working on simulations for v-HES and analysis codes for v-HES can be prepared well before the beamtime.

7. Beam line and beam diagnose (incl. SLI, target viewer etc.)
   ⟶ Contact: **S. Nagao** (Univ. of Tokyo), sho.nagao@nex.phys.s.u-tokyo.ac.jp

   We need detailed discussion with JLab engineers and accelerator experts. Especially, stray magnetic field around the beam pipes between two PCS magnets may affect the primary electron beam and careful beam pipe design and diagnose system are essential for safe beam operation.

Bibliography

[1] B.P. Abott *et al*. (LIGO and VIRGO collaboration), Phys. Rev. Lett. **119**, 161101 (2017).

[2] B.P. Abott *et al*. (LIGO and VIRGO collaboration), Phys. Rev. Lett. **121**, 161101 (2018).

[3] T.E. Riley *et al*., ApJL **887**, L21 (2019).

[4] T.E. Riley *et al*., ApJL **918**, L27 (2021).

[5] JLab Hypernuclear Collaboration, PR12-13-002 submitted to JLab PAC40.

[6] A. Esser, S. Nagao, F. Schulz *et al*., Phys. Rev. Lett. **114**, 232501 (2015).

[7] T.O. Yamamoto *et al*., Phys. Rev. Lett. **90**, 23 (2003).

[8] T. Miyoshi *et al*., (HNSS Collaboration) Phys. Rev. Lett. **90**, 232502 (2003).

[9] L. Yuan *et al*., Phys. Rev. C **73**, 044607 (2006).

[10] S.N. Nakamura *et al*. (HKS Collaboration), Phys. Rev. Lett. **110**, 012502 (2013).

[11] L. Tang *et al*. (HKS Collaboration), Phys. Rev. C **89**, 034320 (2014).

[12] T. Gogami *et al*. (HKS Collaboration), Phys. Rev. C **93**, 034314 (2016).

[13] T. Gogami *et al*. (HKS Collaboration), Phys. Rev. C **94**, 021302(R) (2016).

[14] T. Gogami *et al*. (HKS Collaboration), Phys. Rev. C **103**, L041301 (2021).

[15] G.M. Urciuoli *et al*., Phys. Rev. C **91**, 034308 (2015).

[16] M. Iodice, *et al*., Phys. Rev. Lett. **99**, 052501 (2007).

[17] F. Cusanno, *et al*., Phys. Rev. Lett. **103**, 202501 (2009).

[18] F. Garibaldi *et al*., Phys. Rev. C **99**, 054309 (2019).

[19] T. Gogami *et al*., Proposal to JLab PAC49, **E12-19-002** (2021).

[20] S.N. Nakamura *et al*., Proposal to JLab PAC44, **E12-15-008** (2016).

[21] F. Garibaldi *et al*., Proposal to JLab PAC48, **E12-20-013** (2020).

[22] T. Toyoda, *Basic design of gas target for high accuracy mass measurement of hypertriton at JLab*, Master's Thesis, Kyoto University (2021).

[23] T. Gogami *et. al.*, AIP Conf. Proc. **2319**, 080019 (2021).

[24] T. Gogami *et. al.*, *High accuracy spectroscopy of 3- and 4-body* Λ *hypernuclei at Jefferson Lab*, EPJ Web. Conf. **in Press** (2022).

[25] Y. Fujii *et al.*, Nucl. Instrum. Methods, Phys. Res. Sect. A **795**, 351–363 (2015).

[26] T. Gogami *et al.*, Nucl. Instrum. Methods, Phys. Res. Sect. A **729**, 816–824 (2013).

[27] T. Gogami *et al.*, Nucl. Instrum. Methods, Phys. Res. Sect. A **900**, 69–83 (2018).